Available online at www.sciencedirect.com
SCIENCE DIRECT
ELSEVIER
Ultramicroscopy 106 (2006) 800–807
ultramicroscopy
www.elsevier.com/locate/ultramic

A femtogram resolution mass sensor platform, based on SOI electrostatically driven resonant cantilever. Part I: Electromechanical model and parameter extraction

J. Teva[a,*], G. Abadal[a], F. Torres[a], J. Verd[a], F. Pérez-Murano[b], N. Barniol[a]

[a]*Dept. d'Enginyeria Electrònica, Universitat Autònoma de Barcelona, Bellaterra E- 08193, Spain*
[b]*Institut de Microelectrònica Barcelona (IMB-CNM) Campus UAB, Bellaterra E-08193, Spain*

Received 3 October 2005; accepted 23 December 2005

Abstract

A microcantilever based platform for mass detection in the femtogram range has been integrated in the doped top silicon layer of a SOI substrate. The on-plane fundamental resonance mode of the cantilever is excited electrostatically and detected capacitively by means of two parallel placed electrodes in a two port configuration. An electromechanical model of the cantilever–electrodes transducer and its implementation in a SPICE environment are presented. The model takes into account non-linearities from variable cantilever–electrode gap, fringing field contributions and real deflection shape of the cantilever for the calculation of the driving electrostatic force. A fitting of the model to the measured S_{21} transmitted power frequency response is performed to extract the characteristic sensor parameters as Young modulus, Q factor, electrical parasitics and mass responsivity.

PACS: 77.65.Fs; 83.85.Gk; 85.40.Ux; 07.10.Cm

Keywords: NEMS; Cantilever based sensors; Resonance frequency; Electromechanical model

1. Introduction

Resonating mechanical structures electrically actuated and detected have become one of the key elements of the so-called micro and nano electromechanical systems (MEMS and NEMS). One of the simplest resonating structures is the cantilever, which is the basis of the well-known cantilever based sensors (CBS) [1]. Their unique combination of transducing properties, high quality factor and scalability to nanometer scale dimensions, provide to these sensors with extremely high sensitivities [2] and with a wide range of sensing domains [3]. In these systems, although piezoelectric–optical combination is the more commonly used strategy to excite and detect cantilever vibrations, an electrostatic–capacitive scheme is demonstrated to be the most suitable in terms of nanometer range scalability and CMOS integrability [4,5]. The same electrostatic–capacitive excitation–detection scheme has been also demonstrated to be the most convenient for system oriented applications as resonant RF-MEMS, where acoustic longitudinal modes are excited on stiffer mechanical structures than simple cantilevers [6].

During the design stage of such systems, two problems have to be specifically addressed. From one hand, the electromechanical characterization of the transducer element is crucial for the design of the read-out circuitry and for the optimization of the overall system. This means that the most realistic model for the electromechanical behaviour description has to be provided, as well as the corresponding values of the model parameters, material Young Modulus, structure Q-factor and parasitic electrical elements. From another hand, a functional characterization and calibration of the sensor has also to be performed at the end of the development process. To do that, specific techniques and procedures for cantilever functionalization

*Corresponding author. Tel.: +34 93 581 3514; fax: +34 93 581 2600.
E-mail address: Jorge.Teva@uab.es (J. Teva).

0304-3991/$ - see front matter © 2006 Elsevier B.V. All rights reserved.
doi:10.1016/j.ultramic.2005.12.016

[7] or analyte local deposition [8] have to be developed in parallel and tested on final devices.

In this work we present a mass sensor platform based on a two port electrostatically excited cantilever which resonance can be detected externally without any additional buffer circuitry. The cantilevers together with the excitation-detection electrodes are fabricated on SOI substrates using a single mask optical lithography step. Both, measurement set-up and fabrication simplicity provide robustness and availability to the platform with the device. This is needed to be used for systematic test of cantilever functionalization procedures and for electromechanical model validation and parameter values extraction. A description of the electromechanical model, including equations and approximation assumptions, are provided. The model is implemented in the electrical domain of a SPICE-based simulator, by using special *analog behavior model* (ABM) blocks and electro-mechanical equivalent variables. Compared to other possible alternatives like AHDL based descriptions, SPICE implementation provides more simplicity and portability to PC-based electrical simulation platforms. Finally, magnitude and phase curves of the S_{21} parameter of transmitted signal through the two port cantilever–driver transducer, measured at different excitation voltages have been fitted with the electromechanical model, and from the best fit, model parameters as doped silicon Young modulus, Q factor and parasitic capacitances are extracted. A complete characteristics datasheet of the mass sensor platform is finally provided, including cantilever mechanical properties, electrical parasitics of the overall set-up and expected mass responsivity ($\Re = df/dm$) of the sensor.

2. Experimental

Crystalline silicon cantilevers 40 μm long (l) and 2.3 μm wide (w) have been fabricated on SOI substrates with $h = 5\,\mu m$ thick top silicon and 2 μm thick silicon oxide. As it is shown in the SEM image of Fig. 1a, two electrodes are integrated parallel to the cantilever at a distance $s = 2.4\,\mu m$, for driving (DE) and reading (RE) on plane vibrations corresponding to the lateral fundamental mode. In order to assure good electrical contact when using test probes, top silicon structural layer of SOI has been n-doped with $POCl_3$. After doping, a single photolithography step has been used to define cantilever and driving-sensing electrodes, as well as their corresponding $100 \times 100\,\mu m^2$ contact pads for probe card contacting, on a previously deposited resist layer. This layer is then used as a mask to transfer the transducer patterns to the top SOI structural layer by deep reactive ion etching (DRIE). Finally, cantilevers are released by etching the silicon oxide underneath by means of HF vapours in order to avoid collapse of the structures to the lateral electrodes.

In Fig. 1b, the two port electrical configuration is schematically described. The ac output signal from a network analyzer (Agilent E5100A) is applied to one of the ports of the transducer (DE-CE) which is electrostatically driving the vibrations of the cantilever. The dc voltage applied to the vibrating cantilever, generates an ac current through the output port (CE-RE) which is detected at the input port of the network analyzer. This two port configuration allows to independently applying the dc

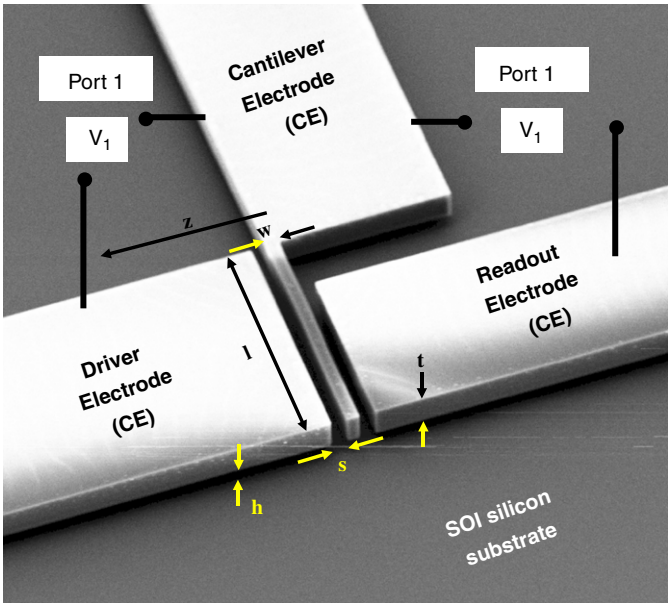

(a)

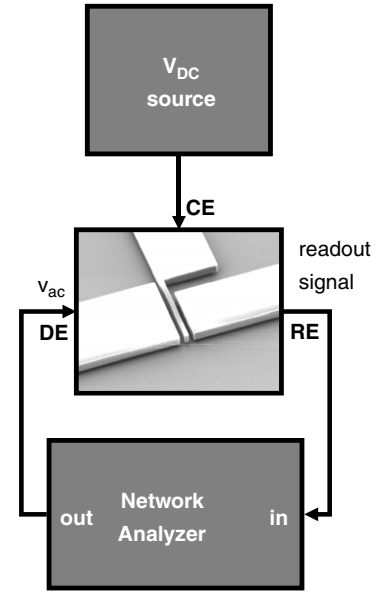

(b)

Fig. 1. (a) SEM image of the cantilever and two electrodes transducer showing the geometrical parameters: length (l), width (w), thickness (h) and cantilever-driver gap distance (s). (b) Block diagram of the two-port configuration. Input port is defined by the driver–electrode (DE) and cantilever–electrode (CE) is used to electrotatically excite the vibration of the cantilever. The read-out current induced at the output port (CE-RE) by the cantilever vibrations and VDC is measured by means of a network analyzer.

and the ac excitation voltage components and minimizing the direct parasitic coupling between input and output ports of the transducer [9]. Using this configuration, the frequency response of the S_{21} transmitted power parameter is systematically measured at different dc cantilever polarization voltages.

In order to obtain a direct measurement of the E/ρ ratio (Young modulus/density) of our structural layer (doped crystalline silicon) we have measured the frequency response of the cantilever mechanical vibration amplitude by exciting with a piezoelectric element based system and detecting the oscillations through an optical microscope. Mechanical excitation of the on plane fundamental mode of the cantilever is accomplished by attaching the SOI chip to the surface of a PZT ceramic which is forced to vibrate in a shear mode [10]. From the measured mechanical vibration frequency response, the resonance frequency without electrostatic forces applied, $f_{res,0V}$, can be determined. Then, from $f_{res,0V}$ and from SEM measured dimensions of the cantilever (w,l), E/ρ ratio can be derived using the following equation:

$$f_{res,0V} = \frac{(1.875)^2}{2 \cdot \pi \cdot \sqrt{12}} \sqrt{\frac{E}{\rho}} \cdot \frac{w}{l^2}. \tag{1}$$

All measurements are performed at ambient pressure, so the main contribution to the Q factor will be air damping of the cantilever.

3. Electromechanical model

The cantilever–driver-system (CDS) modelization presented in this paper is basically based on the model previously published [11]. That model allowed fitting experimental mechanical resonance curves by adding some properties to the traditional lumped model construction [12]. However, electrical output levels have to be confirmed in order to validate the modelization, giving more information to the circuitry design stage. The conception of the model arises from a lumped model approximation, which assures to have convergence on the dynamic solution (not so common in FEM environments), but adding two main features in order to be closed to the real CDS behaviour: (i) the first feature is that the model takes into account the cantilever real deflection, by means of a previous static FEM simulations: (ii) the second feature is considering the effect of the fringing fields on the transducer structure.

3.1. Mechanical-model

The mechanical equation of the cantilever-electrodes transducer consists on the Newton's equation of movement in one dimension for an externally forced and non-linear damped oscillator:

$$m_{eff}\,\ddot{z} + D \cdot \dot{z} + k \cdot z = F_{E-ff}(z,t), \tag{2}$$

where m_{eff} is the cantilever effective mass, that for the first resonant mode can be written as [13]

$$m_{eff} = \rho \cdot l \cdot h \cdot w \cdot \frac{3}{(1.875)^4}, \tag{3}$$

where ρ is the cantilever material mass density.

k is the equivalent stiffness constant of the cantilever [14]:

$$k = \frac{E \cdot h \cdot w^3}{4 \cdot l^3}, \tag{4}$$

and, finally, D is the damping factor, which is related with the damping losses, and hence with the quality factor, Q:

$$D = \frac{\sqrt{k \cdot m_{eff}}}{Q}. \tag{5}$$

The mechanical natural resonance frequency of the fundamental resonant mode can be calculated from k and m_{eff}, by the equation:

$$f_{res,0V} = \frac{1}{2\pi} \sqrt{\frac{k}{m_{eff}}}, \tag{6}$$

re-obtaining Eq. (1).

Non-linear terms due to non-linear stiffness of the cantilever are not considered. That term, characteristic in rigid structures like lateral bridges [14] and transversal cantilevers [6], are not relevant in long cantilever (40 μm) with maximum lateral displacements of about 2 μm [15].

The external forces applied to the cantilever are considered in the term F_{E-ff}. For a cantilever electrostatically coupled with two electrodes (DE and RE), the total external force has to include these two contributions. In terms of the electrical field applied from each electrode, we define the voltage that conforms each electrode with the cantilever electrode, as, (see Fig. 1a):

$$\begin{aligned} V_1(t) &= V_{CE}(t) - V_{DE}(t), \\ V_2(t) &= V_{CE}(t) - V_{RE}(t). \end{aligned} \tag{7}$$

The term of the external forces F_{E-ff} takes into account the two main features above presented: the cantilever real deflection shape and the fringing field correction. Focusing in the real deflection consideration, the model calculates the external electrical force applied to the cantilever by slicing the cantilever length in N components and computing the time-variable capacitance of each sliced element. For each port, the electrostatic force expression obtained is

$$\begin{aligned} F_{E_2^1}(z,t) &= \frac{V_{1_2}(t)^2}{2} \cdot \frac{\partial C_{1_2}}{\partial z} \\ &= \mp \frac{V_{1_2}(t)^2}{2} \cdot \left(\frac{C_0}{s} \sum_{i=1}^{N} \left(\frac{l_i \cdot b_i}{(1 \pm b_i z/s)^2} \right) \right) \end{aligned} \tag{8}$$

where the subindexes 1 and 2 refers to port 1 and port 2, respectively.

The sign convention used in Eq. (6) is shown in Fig. 1a, where the capacitance between cantilever and driver

electrode (port 1) increases as the cantilever bends in the z positive direction.

C_0 is the parallel capacitance in equilibrium between the cantilever and one driver, and is defined as

$$C_0 = \frac{\varepsilon_0 \cdot h \cdot w}{s}, \tag{9}$$

ε_0 is defined as the vacuum permittivity, and l_i and b_i are is the cantilever length and the normalized lateral displacement (on the lateral direction) of the sliced element i, respectively. Those lateral displacements are obtained from previous calculation on a FEM solver platform [16].

The fringing field correction is modelized by an analytical equation which depends only on the cantilever–driver geometry. That term is inspired from a semi-empirical formulation developed to determine the fringing field contribution to adjacent lines in a CMOS circuitry [17]. Then, the total electrostatic force applied to the cantilever can be written as:

$$F_{E-ff_2^1}(z,t) = F_{E_2^1}(z,t)\left(1+\alpha\left(\frac{s}{h}\right)\left(\frac{w}{s}\right)^{0.222}\right), \tag{10}$$

introducing the fringing field factor (α) in order to adjust this contribution to the cantilever–electrodes transducer.

3.2. Electrical model

One of the aims of this paper is to implement this model in an electric circuit simulation environment. In order to do that, the mechanical equation of the system (equation (2)) has to be transformed to the electrical domain. The conversion chosen is the following:

$$F_E \overset{T}{\leftrightarrow} U_E = \frac{F_E}{T}; \quad \dot{z} \overset{T}{\leftrightarrow} I_v = T \cdot \dot{z}, \tag{11}$$

where the external force (F_E) has been transformed to an external voltage in the new domain, and the velocity ($\dot{z}$) has been transformed to an equivalent current (I_v). The factor which defines the transformation between the two domains is given by the equation:

$$T = \frac{C_0}{s} U_R \left[N \Big/ V\right], \tag{12}$$

where C_0 is defined in Eq. (9) and s is the lateral gap between the cantilever and the driver electrode.

U_R is a transformation voltage, where we have considered $U_R = 1\,V$. By this transformation, it is possible to obtain the electrical equivalent for the position (z) and acceleration ($\ddot{z}$):

$$z = \int_0^t \dot{z}\,dt = \frac{1}{T}\int_0^t I_V\,dt, \tag{13}$$

$$\ddot{z} = \dot{I}_v \cdot T. \tag{14}$$

Then the mechanical equation (2) of the cantilever–electrodes system is re-written to its electrical one:

$$L\dot{I}_v + RI_v + \frac{1}{C}\int_0^t I_v\,dt = U_{Eff-1} + U_{Eff-2}. \tag{15}$$

Defining the electrical equivalent parameters:

$$L = \frac{m_{\text{eff}}}{T^2}; \quad C = \frac{T^2}{k}; \quad R = \frac{\sqrt{k \cdot m_{\text{eff}}}}{Q \cdot T^2}. \tag{16}$$

These equivalent electrical parameters are the same as found in the literature [6,9], with the voltage transformation normalized to 1 V.

The equivalent potentials $U_{\text{Eff}-1}$ and $U_{\text{Eff}-2}$ are the force applied to the cantilever by each one of the drivers transformed to the electrical domain, and are obtained by combining Eqs. (10–12) :

$$U_{Eff_2^1}(z,t) = \mp\frac{V_{1_2}(t)^2}{2}\cdot\left(\frac{1}{l}\sum_i\left(\frac{l_i \times b_i}{\left(1 \pm (b_i \cdot z)/s\right)^2}\right)\right) \times\left(1+\alpha\left(\frac{s}{h}\right)\left(\frac{w}{s}\right)^{0.222}\right). \tag{17}$$

The currents I_1 and I_2 generated at each port of the cantilever-electrodes system can be expressed as [11]:

$$I_{1_2} = \dot{V}_{1_2}(t)\frac{C_0}{l}\sum_{i=1}^{N}\frac{l_i}{\left(1 \pm (b_i z)/s\right)} \mp I_v \cdot V_{1_2}(t)\cdot\frac{1}{l}\cdot\sum_{i=1}^{N}\frac{l_i \cdot b_i}{\left(1 \pm (b_i z)/s\right)^2} \tag{18}$$

3.3. Implementation in spice

The electrical equation of movement (Eq. (15)) with the external potential term represented by Eq. (17), and the current generated at the electrodes (Eq. (18)) have been solved in the electrical design environment SPICE [18]. Fig. 2 shows the electrical connections performed to each electrode. The cantilever is driven to resonance by applying an ac signal to the driver electrode combined with the dc voltage applied to the cantilever electrode. The readout electrode is connected directly to the input port of the network analyzer, whose equivalent circuit is depicted in Fig. 2. The modelization takes into account the input impedance of the network analyzer port. This impedance is modelized by a resistor and a capacitor in parallel. The value of the capacitor is adjusted to reproduce the magnitude levels measured out of resonance, and the value of the resistor is fixed to be 1 MΩ. The difference of voltage between the readout and cantilever electrodes ensures the apparition of current at the cantilever resonance. Fig. 3 shows a schematic based on block diagrams of the model implemented in SPICE. In SPICE, the functionality of each block is implemented by ABM modules. The core structure of the model is represented by the RLC branch and the lateral displacement (z) is derived from the voltage drop in the motional capacitor of this RLC branch:

$$\frac{C_0}{s}\cdot U_R = \frac{C}{z}\cdot V_C, \tag{19}$$

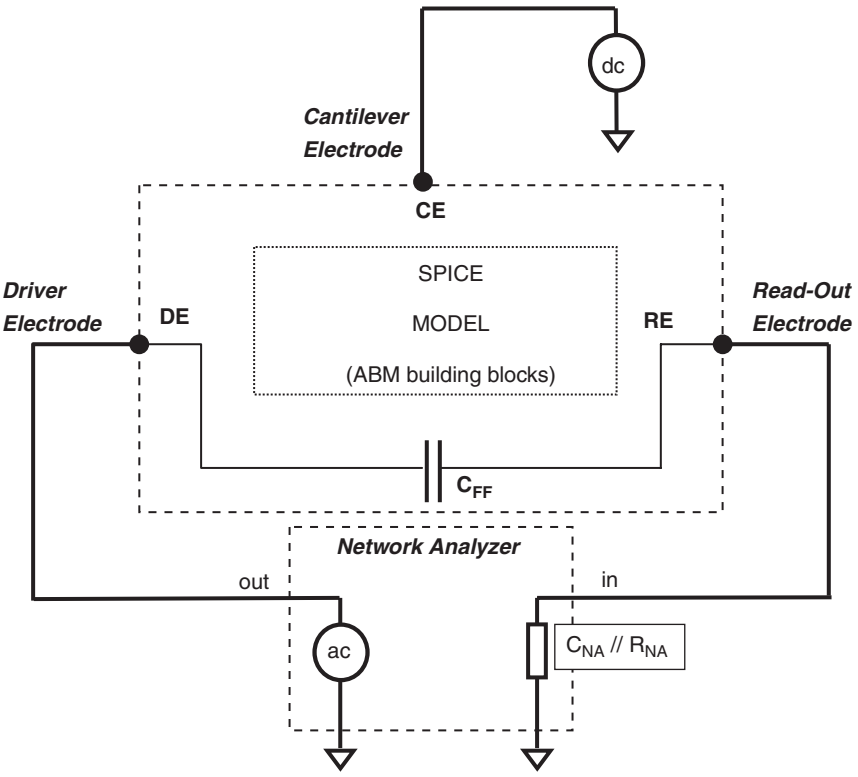

Fig. 2. Scheme showing the electrical connections to the driver, read-out and cantilever electrodes.

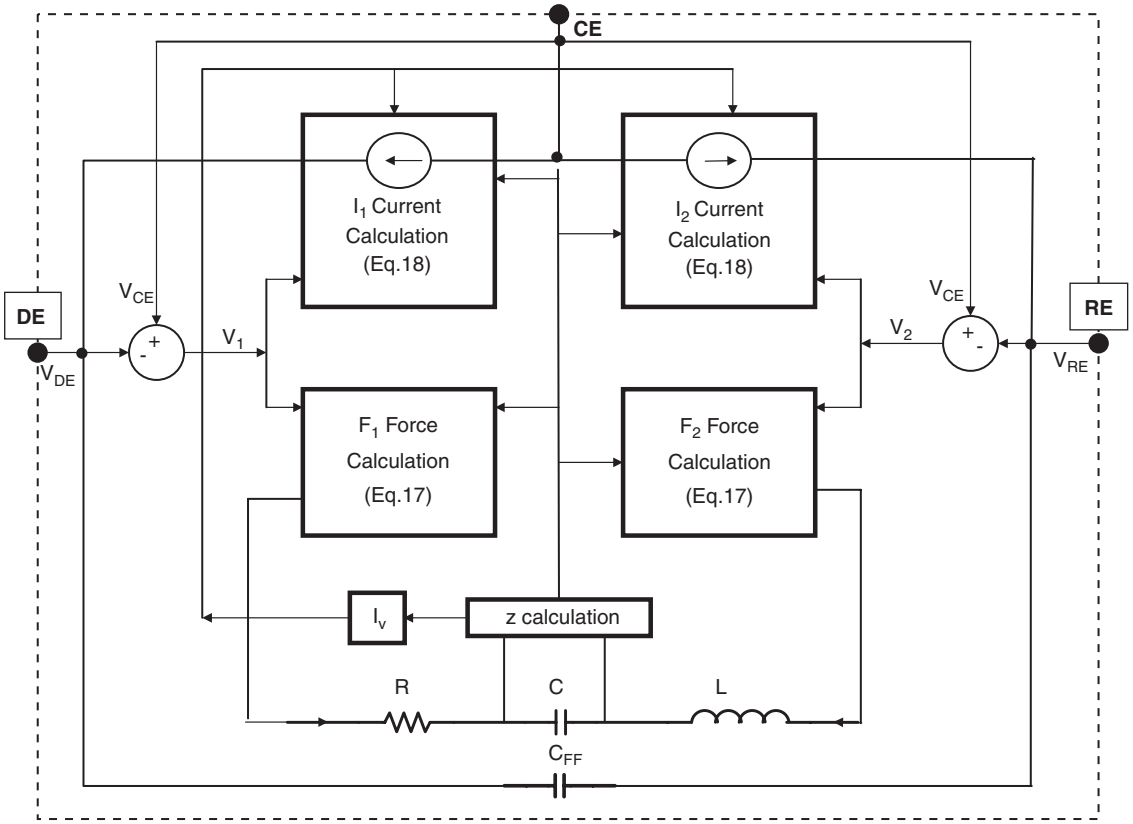

Fig. 3. SPICE schematics implementation of the electromechanical model equations.

where V_C represents the voltage drop at the series capacitance (C). This variable feeds up the current and force modules determining the current (Eq. (18)) generated at both electrodes and the forces (Eqs. (17)) applied to the cantilever. The new force obtained determines the current level at the RLC branch (I_v), obtaining again a new value of the lateral displacement (z). Using this feedback, the electrical Eq. (15) is solved. The current I_v is obtained by integrating the lateral displacement as shown in Eq. (13) (see Fig. 3). This variable feeds the calculation of the current generated at each electrode. Also, the module that calculates the current at each port needs the variable z and the voltage applied at the port. In the same way, the module which calculates the force (Eq. (17)) has to have two inputs, z and the voltage associated to the port, as can be seen in Fig. 3. The modelization is completed by adding a capacitance between the driver and readout electrodes considering the effects of the fringing field that appears between the two ports.

4. Results and discussion

A preliminary measurement has been performed on an SOI chip containing cantilever mass sensor platforms to determine E/ρ ratio of the doped crystalline silicon, using the technique described in Section 2. In Fig. 4, the frequency response of the free (0 V) oscillation amplitude obtained by applying this method is shown. From the central frequency and width of a Lorentzian fit to the experimental points, 0 V resonance frequency and Q factor are obtained:

$$f_{\mathrm{res,0V}} = 490 \pm 2\,\mathrm{kHz},$$

$$Q = 160 \pm 20.$$

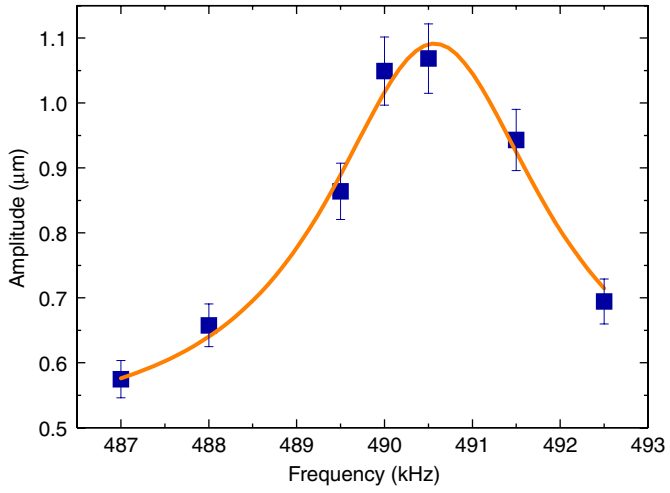

Fig. 4. Measured frequency response of the mechanical oscillation amplitude of the cantilever, around the fundamental on-plane resonance mode, and fit to a Lorentzian curve. Oscillations are excited by attaching the chip to a PZT ceramic which vibrates in a shear mode parallel to the chip plane.

As has been detailed before, from $f_{\mathrm{res,0V}}$ and dimensions of the cantilever ($l = 40\,\mu\mathrm{m}$ and $w = 2.3\,\mu\mathrm{m}$), E/ρ ratio is determined to be $E/\rho = 51.5 \times 10^6\,\mathrm{m^2/s^2}$. Assuming that density of doped crystalline silicon is $\rho = 2.33 \times 10^3\,\mathrm{kg/m^3}$, it gives a Young modulus value of:

$$E = 120\,\mathrm{GPa},$$

which is in accordance to possible values of n-doped crystalline silicon reported previously in the literature [19].

On the other hand, S_{21} parameter measurements using the two port configuration (Fig. 1b) have been performed in order to validate the model and to extract the rest of parameters that characterize the cantilever based sensor platform. In Fig. 5, the measured magnitude (a) and phase (b) of the S_{21} transmitted power parameter through the device at three different V_{DC} cantilever polarization conditions are shown. In all cases, the power of the ac voltage signal injected from the network analyzer to the

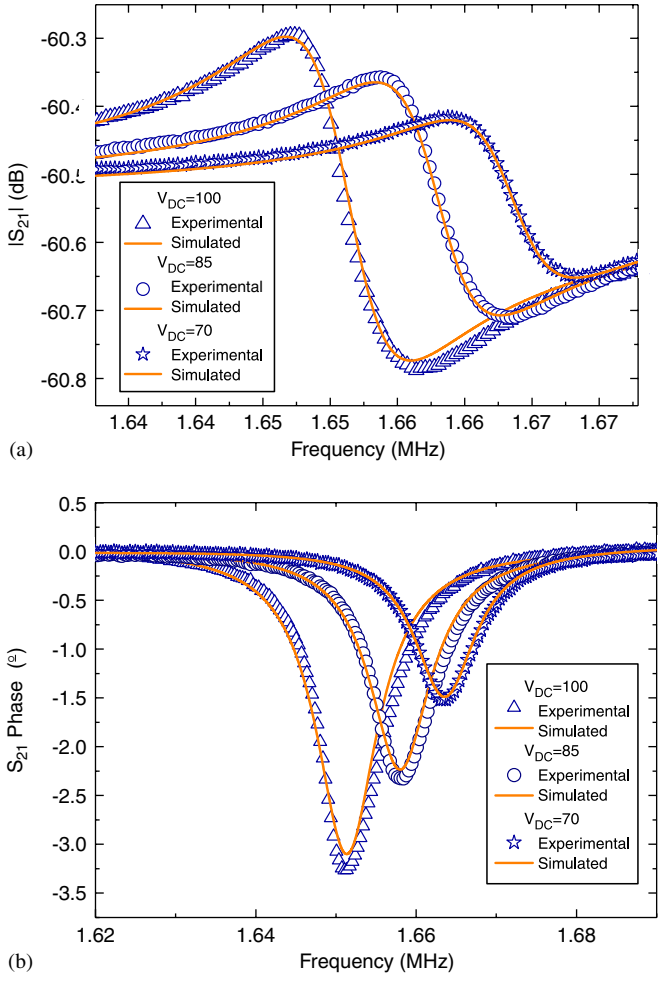

Fig. 5. Magnitude (a) and phase (b) of the S_{21} transmission power parameter measured according to the two-port configuration of Fig. 1b three different cantilever polarization conditions: $V_{DC} = 70\,\mathrm{V}$, $V_{DC} = 85\,\mathrm{V}$ and $V_{DC} = 100\,\mathrm{V}$. In all cases input excitation power is $P_{in} = 18\,\mathrm{dBm}$. Continuous curves correspond to the best fit of the electromechanical model, which parameterized by the following values: $Q = 180$, $E = 120\,\mathrm{GPa}$, $\rho = 2.33 \times 10^3\,\mathrm{kg/m^3}$, $C_{FF} = 22\,\mathrm{fF}$ and $C_{NA} = 23.4\,\mathrm{pF}$, $\alpha = 0.5$.

input port of the transducer is $P_{in} = 18\,\text{dBm}$. The measured transmission signal frequency responses are fitted by the electromechanical model described in Section 3, through SPICE simulations performed using the same polarization and excitation power conditions used in measurements. Fig. 5 also shows the model simulation curves corresponding to the best fit parameters, which are summarized in Table 1. Mainly, once density of doped silicon ($\rho = 2.33 \times 10^3\,\text{kg/m}^3$) and dimensions of the cantilever are fixed, then fit parameters are reduced to Young modulus (E), Q factor (Q), fringing capacitance between driver and readout electrodes (C_{FF}), network analyzer input capacitance (C_{NA}) and fringing field factor for cantilever–driver force calculation (α). From the material and air damping point of view, $E = 120\,\text{GPa}$ and $Q = 180$ values are consistent with our mechanical excitation measurements (Fig. 3) and with other values measured previously [19]. In particular, an enhancement from Q factors of 50–70 measured in doped polysilicon cantilevers [20] is expected by fabricating crystalline silicon cantilevers with similar dimensions. Values of the electrical parameters obtained from best fit, $C_{FF} = 22\,\text{fF}$ and $C_{NA} = 23.4\,\text{pF}$, are also consistent with fringing coupling measurements reported in other similar two port MEMS resonators [14] and with the combined input capacitance of network analyzer and connection wires. A fringing field factor value of $\alpha = 0.5$ is larger compared to $\alpha = 0.02$ obtained previously with poly Si cantilevers 1 μm wide [21]. However, this is consistent with a larger fringing field contribution produced by a wider cantilever ($w = 2.3\,\mu\text{m}$).

Finally, and once the model has been validated and their characteristic parameters have been extracted, the mass responsivity of the cantilever can be deduced from following equation:

$$\Re^{-1} = -\frac{2 \cdot m_{\text{eff}}}{f_{\text{res,0V}}}, \tag{20}$$

which corresponds to the fundamental on plane mode of resonance and assumes that the mass of the analyte is deposited locally at the free end of the cantilever. So, if the resonance frequency of the cantilever is $f_{\text{res,0V}} = 1.6\,\text{MHz}$ and its corresponding effective mass is $m_{\text{eff}} = 2.6 \times 10^{-13}\,\text{kg}$, then mass responsivity value is:

$$\Re^{-1} = 0.3\,\text{fg/Hz}.$$

This mass responsivity value gives a mass resolution between 25 and 108 fg taking into account that the minimum frequency resolution varies between 100 and 360 Hz, depending on the mass measurement time scale [22].

5. Conclusions

A resonant microcantilever with a two-port configuration for electrostatic excitation and capacitive detection is the core transducer of the mass sensor presented in this paper. An electromechanical model of the cantilever–electrodes transducer has been described. The model is implemented in a SPICE electrical environment, which easily allows including external circuitry in the whole sensor simulations. Fit of the model to the measured S_{21} transmitted power frequency response allows, from one hand, validating the model and, from the other hand, extracting model parameters that characterize the sensor. From these parameters, the expected mass responsivity of the sensor is determined to be 0.3 fg/Hz. Single mask

Table 1

Parameter		Value	Units
l	Cantilever length	40	μm
w	Cantilever width	2.3	μm
s	Cantilever–electrodes gap	2.4	μm
h	Cantilever thickness	5	μm
Q	Cantilever quality factor	180	
ρ	Doped crystalline silicon density	2.33×10^3	kg/m^3
E	Doped crystalline silicon Young modulus	120	GPa
m_{eff}	Cantilever effective mass of the fundamental on plane mode	2.6×10^{-13}	kg
k	Cantilever spring constant	28.6	N/m
$f_{\text{res,0V}}$	Cantilever resonance frequency of the fundamental on plane mode with no electrostatic interaction	1.6	MHz
V_{SI}	Lateral snap-in voltage	550	V
V_{DC}	Maximum operating dc voltage	>100	V
P_{in}	Operating power at the input transducer port	18	dBm
R	Series resistance of the SPICE lumped model	161	GΩ
L	Series inductance of the SPICE lumped model	2.7	MH
C	Series capacitance of the SPICE lumped model	3.2	zF
C_{FF}	Fringing coupling capacitance between driving and readout electrodes	22	fF
C_{NA}	Equivalent capacitance at the input network analyzer port	23.4	pF
α	Fringing field factor for cantilever-driver force calculation	0.5	
R_{NA}	Equivalent resistance at the input network analyzer port	1	MΩ
$\Re^{-1} = \text{d}m/\text{d}f$	Mass responsivity of the cantilever, assuming that analyte mass is deposited locally at the free end of the cantilever	0.3	fg/Hz

fabrication process provides simplicity and high yield to device production. A medium stiffness allows applying polarization voltages high enough to induce readout signals which are detectable without the need of any buffer circuitry. So, in summary, fabrication and operation simplicity and robustness makes the sensor presented in this paper a very suitable platform for testing functionalization strategies of cantilevers, and mass analyte deposition procedures.

Acknowledgements

The authors want to thank Professor Jaume Esteve for providing and processing the SOI wafers. This work has been partially funded by the projects IST-2001-33068 (Nanomass-II) and MYCT-TIC2003-0723 (Nanosys).

References

[1] K.L. Ekinci, M.L. Roukes, Rev. Sci. Instr. 76 (2005) 061101.
[2] K.L. Ekinci, X.M.H. Huang, M.L. Roukes, Appl. Phys. Lett. 84–22 (2004) 4469.
[3] R. Berger, C. Gerber, H.P. Lang, J.K. Gimzewski, Microelectron. Eng 35 (1997) 373.
[4] J. Verd, G. Abadal, J. Teva, M. Villarroya, A. Uranga, X. Borrisé, F. Campabadal, J. Esteve, E. Figueras, F. Pérez-Murano, Z.J. Davis, E. Forsén, A. Boisen, N. Barniol, J. Microelectromech. Systems 14 (3) (2005) 508.
[5] S. Ghatnekar-Nilsson, E. Forsén, G. Abadal, J. Verd, F. Campabadal, F. Pérez-Murano, J. Esteve, N. Barniol, A. Boisen, L. Montelius, Nanotechnology 16 (2005) 98.
[6] T. Mattila, J. Kiihamäki, T. Lamminmaäki, O. Jaakkola, P. Rantakari, A. Oja, H. Seppä, H. Kattelus, I. Tittonen, Sensors Actuators A 101 (2002) 1.
[7] A. Bietsch, J. Zhang, M. Hegner, H.P. Lang, C. Gerber, Nanotechnology 15 (2004) 873.
[8] E. Forsén, G. Abadal, S. Ghatnekar-Nilsson, J. Teva, J. Verd, R. Sandberg, W. Svendsen, F. Pérez-Murano, J. Esteve, E. Figueras, F. Campabadal, L. Montelius, N. Barniol, A. Boisen, Appl. Phys. Lett. 87 (2005) 043507.
[9] J.R. Clark, W.-T. Hsu, C. T.-C. Nguyen, Technical Digest, IEEE International Electron Devices Meeting, San Francisco, CAL, December 11–13 (2000) p. 493.
[10] J. Teva, G. Abadal, X. Jordà, X. Borrisé, Z. Davis, N. Barniol. Proceedings of SPIE vol. 5116: Smart Sensors, Actuators and MEMS. Gran Canaria, Spain, May 19–21 (2003) p. 353.
[11] J. Teva, G. Abadal, Z.J. Davis, J. Verd, X. Borrisé, A. Boisen, F. Pérez-Murano, N. Barniol, Ultramicroscopy 100 (2004) 225.
[12] G. Abadal, Z.J. Davis, B. Helbo, X. Borrisé, R. Ruiz, A. Boisen, F. Campabadal, J. Esteve, E. Figueras, F. Pérez-Murano, N. Barniol, Nanotechnology 12 (2001) 100.
[13] D. Sarid, Scanning Force Microscopy, Oxford University Press, Oxford, ISBN 0-19-509204-X, 1991.
[14] T. Mattila, O. Jaakkola, J. Kiihamäki, J. Karttunen, T. Lamminmaäki, P. Rantakari, A. Oja, H. Seppä, H. Kattelus, I. Tittonen, Sensors Actuators A 97-98 (2002) 497.
[15] Q. Jing, T. Mukherjee and G.K. Fedder Large Deflection Beam Model for Schematic Based Behavioral Simulation in NODAS. Technical Proceedings of 2002 International Conference on Modeling and Simulation of Microsystems. NanoTech 2002—MSM 2002. San Juan, Puerto Rico.
[16] http://bsac.berkeley.edu/cadtools/sugar/sugar.
[17] T.S. akurai, K. Tamaru, IEEE Trans. Electron. Dev. ED-30 2 (1983) 183.
[18] http://www.orcad.com/pspicead.aspx.
[19] B. Bhushan, X. Liu, J. Mater. Res. 12-1 (1997) 54.
[20] Z.J. Davis, G. Abadal, O. Kuhn, O. Hansen, F. Grey, A. Boisen, J. Vac. Sci. Technol. B 18-2 (2000) 612.
[21] J. Teva, G. Abadal, Z.J. Davis, J. Verd, X. Borrisé, A. Boisen, F. Pérez-Murano, N. Barniol, Ultramicroscopy 100 (2004) 225.
[22] J. Teva, G. Abadal, F.Torres, J. Verd, F. Pérez-Murano, N. Barniol, Ultramicroscopy, in press, doi:10.1016/j.ultramic.2005.12.017.